Extensive ro-vibrational analysis of deuterated-cyanoacetylene (DC_3N) from millimeter-wavelengths to the infrared domain

Mattia Melosso[a,*], Luca Bizzocchi[b], Aleksandra Adamczyk[c], Elisabetta Canè[c], Paola Caselli[b], Laura Colzi[d], Luca Dore[a], Barbara M. Giuliano[b], Jean-Claude Guillemin[e], Marie-Aline Martin-Drumel[f], Olivier Pirali[f,g], Andrea Pietropolli Charmet[h], Domenico Prudenzano[b], Víctor M. Rivilla[d], Filippo Tamassia[c,*]

[a] *Dipartimento di Chimica "Giacomo Ciamician", Università di Bologna, Via F. Selmi 2, 40126 Bologna (Italy)*
[b] *Center for Astrochemical Studies, Max Planck Institut für extraterrestrische Physik Gießenbachstraße 1, 85748 Garching bei München (Germany)*
[c] *Dipartimento di Chimica Industriale "Toso Montanari", Università di Bologna, Viale del Risorgimento 4, 40136 Bologna (Italy)*
[d] *INAF-Osservatorio Astrofisico di Arcetri, Largo Enrico Fermi 5, 50125, Firenze (Italy)*
[e] *Univ Rennes, Ecole Nationale Supérieure de Chimie de Rennes, CNRS, ISCR–UMR6226, 35000 Rennes (France)*
[f] *Université Paris-Saclay, CNRS, Institut des Sciences Moléculaires d'Orsay, 91405 Orsay (France)*
[g] *SOLEIL Synchrotron, AILES beamline, l'Orme des Merisiers, Saint-Aubin, 91190 Gif-sur-Yvette, (France)*
[h] *Dipartimento di Scienze Molecolari e Nanosistemi, Università Ca' Foscari Venezia, Via Torino 155, 30172 Mestre (Italy)*

Abstract

Cyanoacetylene, the simplest cyanopolyyne, is an abundant interstellar molecule commonly observed in a vast variety of astronomical sources. Despite its importance as a potential tracer of the evolution of star-forming processes, the deuterated form of cyanoacetylene is less observed and less studied in the laboratory than the main isotopologue. Here, we report the most extensive spectroscopic characterization of DC_3N to date, from the millimeter domain to the infrared region. Rotational and ro-vibrational spectra have been recorded using millimeter-wave frequency-modulation and Fourier-transform infrared spectrometers, respectively. All the vibrational states with energy up to $1015\,cm^{-1}$ have been analyzed in a combined fit, where the effects due to anharmonic resonances have been adequately accounted for. The analysis contains over 6500 distinct transition frequencies, from which all the vibrational energies have been determined with good precision for many fundamental, overtone, and combination states. This work provides a comprehensive line catalog for astronomical observations of DC_3N.

Keywords: Cyanoacetylene, Interstellar species, Ro-vibrational spectroscopy, Spectral analysis, Anharmonic resonances, Line catalog

1. Introduction

Highly unsaturated molecules account for a large portion of the known interstellar species [1]. For instance, the presence of several carbon-chain molecules is one of the most characteristic features of the chemical composition of starless cores, such as the Taurus Molecular Cloud (TMC-1), one of the brightest source of carbon-chain species [2]. Among the unsaturated molecular species, cyanopolyynes, i.e., linear molecules of general chemical formula $HC_{2n+1}N$, are widespread in the interstellar medium (ISM) and all members up to $HC_{11}N$ have been detected to date [3]. Cyanoacetylene (HC_3N, IUPAC name prop-2-ynenitrile), the simplest member of the cyanopolyynes family, was found to be an abundant species in a large variety of astronomical objects: starless cores [4], post-AGB objects [5], carbon-rich circumstellar envelopes

☆Supplementary material available.

*Corresponding authors
Email addresses: mattia.melosso2@unibo.it (Mattia Melosso), filippo.tamassia@unibo.it (Filippo Tamassia)

[6], massive star-forming regions [7], protoplanetary disks [8], solar-type protostars [9], external galaxies [10], and Galactic Center molecular clouds [11].

The deuterated form of cyanoacetylene (DC_3N) has been detected in the ISM as well. The first astronomical observation of DC_3N has been reported towards TMC-1 [12] by the detection of the $J = 5 \rightarrow 4$ emission rotational transition around 42 GHz. Consecutively, DC_3N has tentatively been detected in the high-mass star-forming regions Orion KL [13] and Sagittarius B2 [14]. In these regions, deuterium fractionation is not as effective as in dark clouds, thus preventing a strong enhancement above the deuterium cosmic abundance. Recently, DC_3N has been detected in some low-mass cores (see e.g., Refs.[9],[15]) and in a sample of 15 high-mass star-forming cores [16]. The latter work, based on the spectroscopic results presented in this paper, suggests that DC_3N is enhanced in the cold and outer regions of star-forming regions, likely indicating the initial deuteration level of the large-scale molecular cloud within which star formation takes place. Rivilla *et al.* [16] also summarize all the astronomical observations of DC_3N so far.

Microwave (MW) transitions of DC_3N were first reported for the ground and the four lowest singly-excited states during the course of an extensive study of cyanoacetylene isotopologues [17]. A larger number of vibrationally excited states was re-examined in depth some years later and a rigorous determination of the effective molecular parameters was attained [18]. Recently, the laboratory investigation of the rotational spectrum of DC_3N has been extended to the THz regime for the ground and the $v_7 = 1$ states [19]. In the same paper, the authors revised the ^{14}N and D hyperfine-structure constants derived in Refs. [20, 21] from supersonic-jet Fourier-Transform Microwave (FT-MW) spectroscopy.

As far as its infrared (IR) spectrum is concerned, the experimental position and intensity of all fundamentals but the weak ν_4 mode have been determined from low resolution ($0.5\,cm^{-1}$) studies [22, 23]. Some combination and overtone bands were also observed in the same works. In addition, two medium resolution (0.025–$0.050\,cm^{-1}$) IR studies were performed by Mallinson & Fayt [24] and Coveliers *et al.* [25]. In the former, the band center of the three stretching modes of DC_3N (ν_1, ν_2, and ν_3) has been determined; in the latter, the far-infrared (FIR) spectrum was recorded between 200 and $365\,cm^{-1}$ and the ν_7 fundamental was analyzed together with the bands $\nu_6 - \nu_7$, $\nu_5 - \nu_7$, and $\nu_4 - \nu_6$, and their hot-bands.

In this work, a detailed investigation of both millimeter/submillimeter-wave and infrared spectra of DC_3N is reported. Pure rotational transitions within all the vibrational states with energy lower than $1015\,cm^{-1}$ have been detected and 27 fundamental, overtone, combination, and hot ro-vibrational bands have been analyzed at high resolution (0.001–$0.01\,cm^{-1}$). The new measurements have been combined in a fit containing almost 6700 distinct transition frequencies, thus allowing the determination of a consistent set of spectroscopic parameters. This work represents the most exhaustive spectroscopic characterization of DC_3N so far and provides a robust line catalog useful for astronomical applications. Moreover, the large number of vibrational excited states are of interest for harmonic/anharmonic force field computations.

The paper is structured as follows. First, the synthesis of the sample and the spectrometers used for spectral recording are described (§2). Then, the effective Hamiltonian employed for the energy levels description is given (§3). Successively, the general features of the spectra and their analysis are discussed (§4). Finally, the results are summarized and the conclusions are presented (§5).

2. Experimental details

2.1. Synthesis of deuterocyanoacetylene

Methyl propiolate ($HC{\equiv}CCOOCH_3$) was purchased from TCI-Europe and used without further purification. The DC_3N sample was synthesized in Rennes following the procedure described in Ref. [23]. Briefly, $HC{\equiv}CCOOCH_3$ was added dropwise to liquid ammonia resulting in a 100 % conversion into $HC{\equiv}CCONH_2$. The propiolamide was then mixed with phosphorous anhydride (P_4O_{10}) and calcined white sand; the whole system was heated up to 470 K over 2 h while connected to a liquid nitrogen-cooled trap where pure cyanoacetylene was collected. Cyanoacetylene (3 g), heavy water (D_2O, 4 mL) and potassium carbonate (K_2CO_3, 50 mg) were mixed together in an inert atmosphere. The biphasic mixture was then stirred for about 20 min at room temperature. Subsequently, on a vacuum line, partially deuterated cyanoacetylene was condensed in a 77 K cooled trap, while water was blocked in a first 220 K trap. The operation was

repeated 3 times by addition of D_2O and K_2CO_3 to the partially deuterated cyanoacetylene. The residual D_2O was removed by vaporisation on P_4O_{10} and DC_3N was finally condensed in a trap cooled to 150 K. Deuterocyanoacetylene with an isotopic purity greater than 98 % was obtained in a 67 % yield. The sample can be stored indefinitely at 250 K without decomposition.

2.2. Infrared spectrometers

The FIR spectrum of DC_3N was recorded at the AILES beamline of the SOLEIL synchrotron facility using a Bruker IFS 125 FT interferometer [26] and a white-type multipass absorption cell whose optics were adjusted to obtain a 150 m optical path length [27, 28]. For the present experiment, we used the far-IR synchrotron radiation continuum extracted by the AILES beamline. The interferometer was equipped with a 6 µm Mylar-composite beamsplitter and a 4 K cooled Si-bolometer. Two 50 µm-thick polypropylene windows isolated the cell from the interferometer, which was continuously evacuated to 0.01 Pa limiting the absorption of atmospheric water. Vapor of DC_3N was injected into the absorption cell at a 25 Pa pressure. The spectrum covers the range 70–500 cm^{-1} and consists of the co-addition of 380 scans recorded at 0.00102 cm^{-1} resolution.

IR spectra in the 450–1600 cm^{-1} range were recorded in Bologna using a Bomem DA3.002 Fourier-Transform spectrometer [29]. It was equipped with a Globar source, a KBr beamsplitter, and a liquid nitrogen-cooled HgCdTe detector. A multi-pass cell with absorption-lengths from 4 to 8 m was employed for the measurements. Sample pressures ranging between 25 and 650 Pa were used to record the spectra. The resolution was generally 0.004 cm^{-1}, except for the very weak ν_4 band, which was recorded at a lower resolution of 0.012 cm^{-1}. Several hundreds of scans, typically 800, were co-added in order to improve the signal-to-noise ratio (S/N) of the spectra.

All the spectra have been calibrated using residual water or CO_2 absorption lines whose reference wavenumbers were taken from Refs. [30, 31] and from `HITRAN` [32], respectively. No apodization functions were applied to the interferograms.

2.3. Millimeter and submillimeter spectrometers

Rotational spectra have been recorded using two frequency-modulation (FM) millimeter/submillimeter spectrometers located in Bologna and in Garching.

The Bologna spectrometer has been described in details elsewhere [33, 34]. Briefly, a Gunn diode oscillator operating in the W band (80–115 GHz) was used as primary source of radiation, whose frequency and phase stability are ensured by a Phase-Lock Loop (PLL). Spectral coverage at higher frequencies was obtained by coupling the Gunn diode to passive frequency multipliers in cascade (doublers and triplers, Virginia Diodes, Inc.). The output radiation, sine-wave modulated in frequency (f = 48 kHz), was fed to the glass absorption cell containing DC_3N vapors at a pressure between 1 and 15 Pa, depending on the intensity of the lines under consideration. The outcoming signal was detected by a Schottky barrier diode and sent to a Lock-in amplifier set at twice the modulation-frequency ($2f$ scheme); the demodulated signal is then filtered into a resistor-capacitor (RC) system before data acquisition.

In Garching the CASAC spectrometer developed at the Max-Planck-Institut für extraterrestrische Physik was used. Full details on the experimental set-up are given in Ref. [35]; here, we report only a few key details which apply to the present investigation. The instrument is equipped with an active multiplier chain (Virginia Diodes) as a source of radiation in the 82–125 GHz band. Further multiplier stages in cascade allow to extend the frequency coverage up to $\sim$ 1.1 THz with an available power of 2–20 µW. The primary millimeter radiation stage is driven by a cm-wave synthesizer (Keysight E8257D) operating in the 18-28 GHz band, which is locked to a Rb atomic clock to achieve accurate frequency and phase stabilisation. A closed-cycle He-cooled InSb hot-electron bolometer operating at 4 K (QMC) is used as a detector. As in Bologna, frequency (f = 50 kHz) modulation technique is employed and the second derivative of the actual absorption profile is thus recorded by the computer-controlled acquisition system after lock-in demodulation at $2f$. The absorption cell is a plain Pyrex tube (3 m long and 5 cm in diameter) fitted with high-density polyethylene windows. The measurement were performed using gaseous samples at pressure of a few Pa. In this condition, DC_3N is stable for ca. 2 h without significant decomposition due to hydrogen exchange.

The spectra were recorded in the frequency ranges 80–115 GHz and 920–1070 GHz in Garching, and in the window 240–440 GHz in Bologna.

Table 1: Energy and intensity of all fundamental modes of DC_3N.

Modes	Description	Energy (cm^{-1})	Reference	Abs. intensity ($atm^{-1}cm^{-2}$)
ν_1	C−D stretching	2608.520(3)	[24]	81.3 ± 5.7^{a}
ν_2	C≡C stretching	2252.155(3)	[24]	50.5 ± 2.4^{a}
ν_3	C≡N stretching	1968.329(3)	[24]	38.7 ± 4.0^{a}
ν_4	C−C stretching	867.60(6)	This Work	$< 0.1^{b}$
ν_5	CCD bending	522.263933(7)	This Work	83.8 ± 4.7^{a}
ν_6	CCC bending	492.759896(7)	This Work	$106. \pm 8^{a}$
ν_7	CCN bending	211.550293(5)	This Work	0.89 ± 0.11^{b}

[a] From low-resolution integrated band-intensity measurements at 296 K (Ref. [23]). **[b]** From low-resolution integrated band-intensity measurements at 293 K (Ref. [22]).

3. Theoretical background

From a spectroscopic point of view, DC_3N is a closed-shell linear rotor. It has 7 vibrational modes: 4 stretchings (ν_1–ν_4; Σ symmetry) and 3 doubly-degenerated bendings (ν_5–ν_7; Π symmetry). They are summarized in Table 1. In the present work, only the low-lying vibrational states (v_4, v_5, v_6, and v_7, with one of multiple quanta of excitation) have been investigated for two main reasons: (i) transitions associated to the lower energy states are of astrophysical interest, and (ii) some of the vibrational states are connected by a network of anharmonic resonances fully described within our chosen energy threshold of 1015 cm^{-1}; above this limit the states are either unperturbed or involved in higher-order resonances. Therefore, the stretching modes ν_1, ν_2, and ν_3, lying above this threshold, have not been investigated. Conventionally, we labelled a given vibrational state with the notation $(v_4, v_5^{l_5}, v_6^{l_6}, v_7^{l_7})_{e/f}$, where l_t is the vibrational angular momentum quantum number associated to the bending mode t and the e/f subscripts indicate the parity of the symmetrized wave functions [36]. When the l_t and e/f labels are not indicated, we refer to all the possible sub-levels of a state.

The full ro-vibrational wave-function is then given by the ket $\left|v_4, v_5^{l_5}, v_6^{l_6}, v_7^{l_7}; J, k\right\rangle_{e/f}$. The vibrational part of the wave-function is expressed as combination of one- or two-dimensional harmonic oscillators, whereas the rotational part is the symmetric-top wave-function whose quantum number k is given by $k = l_5 + l_6 + l_7$. A substate is denoted as Σ when $k = 0$, Π for $|k| = 1$, Δ for $|k| = 2$, and so on.

The following Wang-type linear combinations [37] lead to symmetry-adapted basis functions:

$$\left|v_4, v_5^{l_5}\ , v_6^{l_6}, v_7^{l_7}; J, k\right\rangle_{e/f} = \frac{1}{\sqrt{2}}\left\{\left|v_4, v_5^{l_5}, v_6^{l_6}, v_7^{l_7}; J, k\right\rangle \pm (-1)^k \left|v_4, v_5^{-l_5}, v_6^{-l_6}, v_7^{-l_7}; J, -k\right\rangle\right\}\ , \tag{1a}$$

$$\left|v_4, 0^0\ , 0^0, 0^0; J, 0\right\rangle_e = \left|v_4, 0^0, 0^0, 0^0; J, 0\right\rangle\ . \tag{1b}$$

The upper and lower signs ($\pm$) correspond to e and f wave-functions, respectively. For Σ states ($k = 0$), the first non-zero l_t is chosen positive. Here, the omission of the e/f label indicates unsymmetrised wave-functions. The Hamiltonian used to reproduce the ro-vibrational energy levels is equivalent to the one used

for HC_3N [38]:

$$\mathscr{H} = \mathscr{H}_{\rm rv} + \mathscr{H}_{l-{\rm type}} + \mathscr{H}_{\rm res}\,, \tag{2}$$

where $\mathscr{H}_{\rm rv}$ is the ro-vibrational energy including centrifugal distortion corrections, $\mathscr{H}_{l-{\rm type}}$ represents the l-type interaction between the l sub-levels of the excited bending states, and $\mathscr{H}_{\rm res}$ accounts for resonances among accidentally quasi-degenerate ro-vibrational states. The resonance network active in DC_3N resembles the one found for HC_3N and will be described later.

The Hamiltonian matrix is built by using unsymmetrised ro-vibrational functions. It is subsequently factorized and symmetrized using Eqs. (1). The matrix elements of the effective Hamiltonian are expressed using the formalism already employed for the analysis of HC_3N [38].

4. General features and analysis

4.1. Vibrational spectra

Although infrared spectra were recorded up to 1600 $\rm cm^{-1}$ in this study, our analysis is limited to the portion of the electromagnetic spectrum below $\sim$ 1040 $\rm cm^{-1}$. This is because the highest energy state within our threshold of 1015 $\rm cm^{-1}$ is the (0110) state, whose combination band falls in the region 999–1035 $\rm cm^{-1}$. In total, 27 ro-vibrational bands have been observed at high resolution for the first time and successfully analyzed. They include fundamental, overtone, combination, and hot-bands, and are listed in Table 2 along with the observed sub-bands, frequency and J ranges, number of data used in the analysis, and the root-mean-square (*rms*) error of the final fit. All the observed bands are also graphically displayed in Figure 1.

Figure 2 shows a general overview of portions of the FIR (180–460 $\rm cm^{-1}$ range, upper panel) and mid-infrared (MIR, 450–800 $\rm cm^{-1}$ range, bottom panel) spectra recorded in this work. The most prominent bands in the FIR region are the ν_7 fundamental, $\nu_6-\nu_7$, $\nu_5-\nu_7$, $\nu_4-\nu_6$, and $2\nu_7$ overtone bands. The MIR region is dominated by the very strong fundamentals ν_6 and ν_5. The low-frequency side of the spectrum is particularly crowded due to the proximity of the two fundamentals, the presence of their associated hot-bands, and of the ν_6 of HC_3N centered at 500 $\rm cm^{-1}$. HC_3N is present in the sample as result of the H/D exchange in the cell.

Having a medium IR intensity, the combination bands $\nu_6+\nu_7$ and $\nu_5+\nu_7$ are well visible in the high-frequency part of the MIR spectrum as seen in the bottom panel of Figure 2. Although not displayed in Figure 2, the overtone $2\nu_6$ and the combination $\nu_5+\nu_6$ bands centered around 975–1018 $\rm cm^{-1}$ and 999–1035 $\rm cm^{-1}$, respectively, are clearly detectable as well, despite the presence of strong absorption lines due to HDO. The very weak ($<$ 0.1 $\rm atm^{-1}$ $\rm cm^{-2}$) ν_4 fundamental at 830–865 $\rm cm^{-1}$ had to be recorded at higher pressure (400 Pa) and lower resolution (0.012 $\rm cm^{-1}$). In this case, up to 2600 scans were co-added to improve the S/N of the spectrum.

4.2. Rotational spectra

Rotational spectra were recorded for all the 14 states whose vibrational energy do not exceed our threshold of 1015 $\rm cm^{-1}$. Literature data were available for some of these states, as pointed out in Section 1. However, line positions of some millimeter-wave transitions from Ref. [17] are affected by large uncertainties (up to 300 kHz) and many data are limited to low frequencies. For these reasons, we decided to re-investigate and extend the spectrum for all these vibrational states. The largest improvements have been realized for the states (1000), (0110), (0020), and (0004) involved in a network of anharmonic resonances, for which extended data-sets were obtained. In particular, the (0110) state, not included in the analysis of Ref. [18], has been assigned for the first time in this study and its interaction with the (1000) state has been identified and properly accounted for.

Table 3 summarizes the set of rotational data used in the analysis, specifying the observed sub-levels, J and frequency ranges, number of distinct fitted frequencies, the *rms* error of the final fit, and the corresponding references used.

With the exception of $v_4 = 1$, all the states possess a rotational constant B greater than that of the ground state and therefore their rotational lines lie at frequencies higher than those of the corresponding

Table 2: Ro-vibrational bands recorded and analyzed in this work.

Band	Sub-bands	Freq. range (cm^{-1})	J range	No. of lines	$rms \times 10^4$ (cm^{-1})
ν_7	$\Pi - \Sigma^+$	190-240	1-93	258	0.5
ν_6	$\Pi - \Sigma^+$	466-522	2-109	267	3.6
ν_5	$\Pi - \Sigma^+$	500-557	0-117	255	3.7
ν_4	$\Sigma^+ - \Sigma^+$	830-865	0-61	109	9.6
$2\nu_7$	$\Sigma^+ - \Sigma^+$	405-445	2-78	136	1.0
$2\nu_6$	$\Sigma^+ - \Sigma^+$	975-1018	2-101	141	5.2
$\nu_6 + \nu_7$	$\Sigma^+ - \Sigma^+$	686-736	1-89	166	2.5
$\nu_5 + \nu_7$	$\Sigma^+ - \Sigma^+$	715-769	1-105	170	3.0
$\nu_5 + \nu_6$	$\Sigma^+ - \Sigma^+$	999-1035	3-63	102	3.8
$\nu_6 - \nu_7$	$\Pi - \Pi$	257-306	1-89	309	0.6
$\nu_5 - \nu_7$	$\Pi - \Pi$	288-333	1-86	291	0.7
$\nu_4 - \nu_6$	$\Sigma^+ - \Pi$	329-375	1-79	222	0.6
$4\nu_7 - \nu_6$	$\Sigma^+ - \Pi$	351-352	59-60	2	0.4
$2\nu_7 - \nu_7$	$\Sigma - \Pi$	193-236	1-78	391	0.8
$3\nu_7 - 2\nu_7$	$\Pi - \Sigma^+$	191-235	4-77	178	0.7
$4\nu_7 - 3\nu_7$	$\Sigma^+ - \Pi$	193-219	10-58	89	0.9
$3\nu_7 - \nu_7$	$\Pi - \Pi$	405-441	4-68	208	1.0
$\nu_6 + \nu_7 - \nu_7$	$(\Sigma, \Delta) - \Pi$	478-508	5-56	329	6.9
$\nu_6 + 2\nu_7 - 2\nu_7$	$\Pi - (\Sigma^+, \Delta)$	476-512	12-65	93	5.2
$2\nu_6 - \nu_6$	$\Sigma - \Pi$	500-519	10-68	43	7.0
$\nu_5 + \nu_7 - \nu_7$	$(\Sigma^+, \Delta) - \Pi$	505-545	2-75	464	4.5
$\nu_5 + 2\nu_7 - 2\nu_7$	$\Pi - (\Sigma, \Delta)$	505-542	2-82	106	3.5
$\nu_6 + 2\nu_7 - \nu_7$	$\Pi - \Pi$	690-718	4-53	153	4.7
$\nu_5 + 2\nu_7 - \nu_7$	$\Pi - \Pi$	721-748	2-45	296	4.1
$\nu_5 + \nu_7 - 2\nu_7$	$(\Sigma^+, \Delta) - (\Sigma^+, \Delta)$	290-330	2-81	261	0.9
$\nu_6 + \nu_7 - 2\nu_7$	$(\Sigma^+, \Delta) - (\Sigma^+, \Delta)$	256-306	2-84	402	0.9
$4\nu_7 - 2\nu_7$	$(\Sigma^+, \Delta) - (\Sigma^+, \Delta)$	406-437	5-67	302	1.0

ground state transition. This can be seen in Figure 3, where the broad scan covers the $J = 13 \leftarrow 12$ transitions for many vibrational satellites. In this excerpt, the l-type resonance patterns of all the excited bending states analyzed are visible. From a visual inspection, it is easy to associate some of these patterns to the pertaining state: the ground and $v_4 = 1$ exhibit a single line, while each bending state has $\sum = \prod_t (l_t+1)$ lines (even though not always resolvable).

4.3. Analysis of the spectra

The sample of pure rotational and ro-vibrational data contains 6691 distinct frequencies involving 14 vibrational states of DC_3N. This work represents the first-ever investigation of its ro-vibrational spectrum in the region between 365 and 1040 cm^{-1}. Moreover, the FIR spectrum has been thoroughly re-investigated at higher resolution with an accuracy two or three orders of magnitude better than Ref. [25]. As far as the rotational spectrum is concerned, this work extends the observation of excited states transitions to

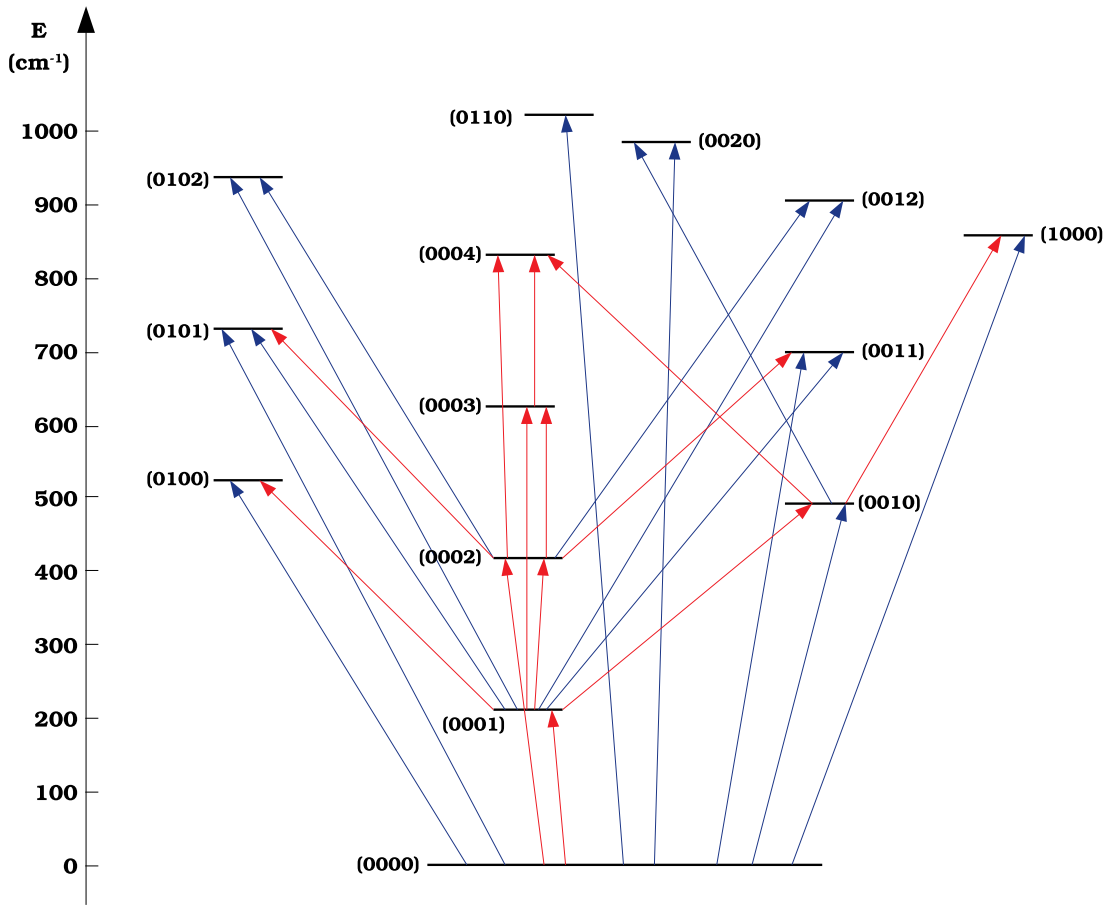

Figure 1: Vibrational energy-level diagram of DC_3N up to 1015 cm^{-1}, where the arrows represent the 27 IR bands analyzed in this work. Red and blue arrows indicate the bands observed at SOLEIL and in Bologna, respectively.

the submillimeter-wave region. In addition, rotational transitions with J up to 126 were recorded at THz frequencies (1.069 THz) although only for the ground state.

In the combined fit, a different weight was given to each datum in order to take into account the different measurements precision. Uncertainties spanning from 0.0004 to 0.00075 cm^{-1} were used for the infrared measurements performed in Bologna; the weak ν_4 band being the only exception, for which an uncertainty of 0.001 cm^{-1} was assumed. FIR data recorded at higher resolution with the FT-IR spectrometer of the AILES beamline have been given uncertainties between 0.00005 and 0.0001 cm^{-1}, based on calibration residuals and the S/N of spectral lines. As far as pure rotational transitions are concerned, we assumed a typical experimental error of 10–20 kHz for our new millimeter/submillimeter measurements. Data from literature were used with the uncertainty stated in the original papers [17, 18, 19]. Only few lines from Ref. [17], whose residuals were far off their declared errors, were not used in the fit.

The spectral analysis was performed using a custom `PYTHON` code that employs the `SPFIT` program [39] as computational core (see Ref. [38] for further details about the code). The data were fitted to the Hamiltonian of Eq. (2) and its coefficients optimized in an iterative least-squares procedure. Some spectroscopic parameters could not be determined from the available experimental data. In these cases, the constant of a given vibrational level were derived from the corresponding optimized values obtained for other

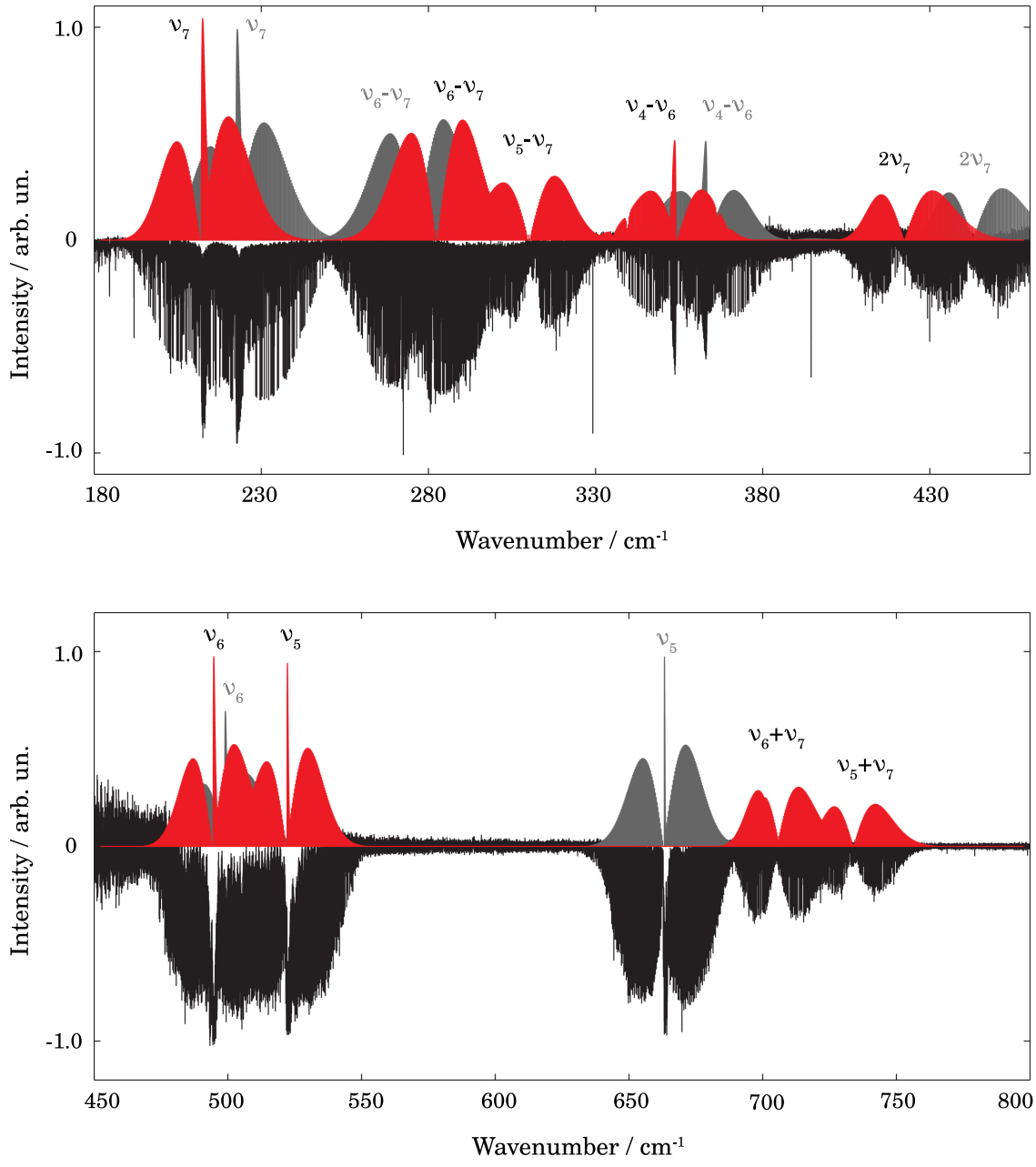

Figure 2: Portions of the FIR (upper panel) and MIR (lower panel) spectra of *d*-cyanoacetylene (black traces). A simulation spectrum of the most intense bands is also reported for both DC_3N (red) and HC_3N (grey). Lines belonging to CO and various H_2O isotopologues were removed from the spectra.

Table 3: Summary of the rotational data used in the analysis.

State	$\|k\|$	J range	Freq. range (GHz)	No. of lines	rms (kHz)	Reference
Ground state	0	3-126	33-1069	52	13.2	TW, Ma78, Pl88, Sp08
$v_7 = 1$	$1_{e,f}$	5-105	50-896	67	10.9	TW, Ma78, Pl88, Sp08
$v_6 = 1$	$1_{e,f}$	7-44	67-381	42	17.0	TW, Pl88
$v_5 = 1$	$1_{e,f}$	7-44	67-381	42	13.7	TW, Pl88
$v_4 = 1$	0	7-51	67-439	32	23.6	TW, Pl88
$v_7 = 2$	$0, 2_{e,f}$	7-44	67-383	61	24.0	TW, Ma78, Pl88
$v_7 = 3$	$(1, 3)_{e,f}$	7-44	68-384	77	20.0	TW, Ma78, Pl88
$v_7 = 4$	$0,(2, 4)_{e,f}$	7-48	68-419	85	19.8	TW, Pl88
$v_6 = 2$	$0, 2_{e,f}$	7-44	67-382	54	44.7	TW, Pl88
$v_6 = v_7 = 1$	$(0, 2)_{e,f}$	7-44	67-382	93	30.8	TW, Ma78, Pl88
$v_5 = v_7 = 1$	$(0, 2)_{e,f}$	7-44	67-382	78	20.8	TW, Pl88
$v_5 = v_6 = 1$	$(0, 2)_{e,f}$	9-44	84-381	63	14.6	TW
$v_6 = 1, v_7 = 2$	$(\pm1, 3)_{e,f}$	7-46	68-400	95	21.9	TW, Pl88
$v_5 = 1, v_7 = 2$	$(\pm1, 3)_{e,f}$	9-44	85-383	97	17.4	TW
interstate[a]		44-49	364-429	10	19.7	TW

Abbreviations are used as follow: **TW** This work, **Ma78** Mallinson & De Zafra (1978) [17], **Pl88** Plummer *et al.* (1988) [18], **Sp08** Spahn *et al.* (2008) [19]. [a] Transitions between the interacting states (1000) and (0004).

Table 4: Spectroscopic constants derived for DC_3N in the ground and $v_4 = 1$ states.

Constant	Unit	Ground state	$v_4 = 1$
G_v	cm^{-1}	0.0	867.594(75)
B_v	MHz	4221.580853(37)	4212.271(16)
D_v	kHz	0.4517857(89)	0.45312(11)
H_v	mHz	0.03949(78)	0.03949[a]
L_v	nHz	−0.154(23)	−0.154[a]

Number in parenthesis are one standard deviation in units of the last quoted digit. [a] Kept fixed to ground state value.

levels belonging to the same vibrational manifold considering, whenever feasible, a vibrational dependence. In other cases, they were simply fixed to zero. The spectroscopic parameters obtained from the combined fit procedure are collected in Tables 4-7.

As anticipated, the analysis of DC_3N follows the approach successfully adopted for HC_3N [38]. The main difference is the set-up of the anharmonic resonances network, which arises from the different energy of some vibrational levels due to the isotopic substitution. In particular, the ν_5 vibrational energy, 663.36848(3) cm^{-1} in HC_3N, drops to 522.26378(2) cm^{-1} in DC_3N. For HC_3N, two resonant systems were described: (i) $v_5 = 1 \sim v_7 = 3$ and ii) $v_4 = 1 \sim v_5 = v_7 = 1 \sim v_6 = 2 \sim v_7 = 4$. Of the two systems, the former is not present in DC_3N while the latter is almost the same, except for $v_5 = v_7 = 1$, replaced by $v_5 = v_6 = 1$. The treatment of such perturbations led to the determination of the corresponding interaction parameters, C_{30} for the cubic

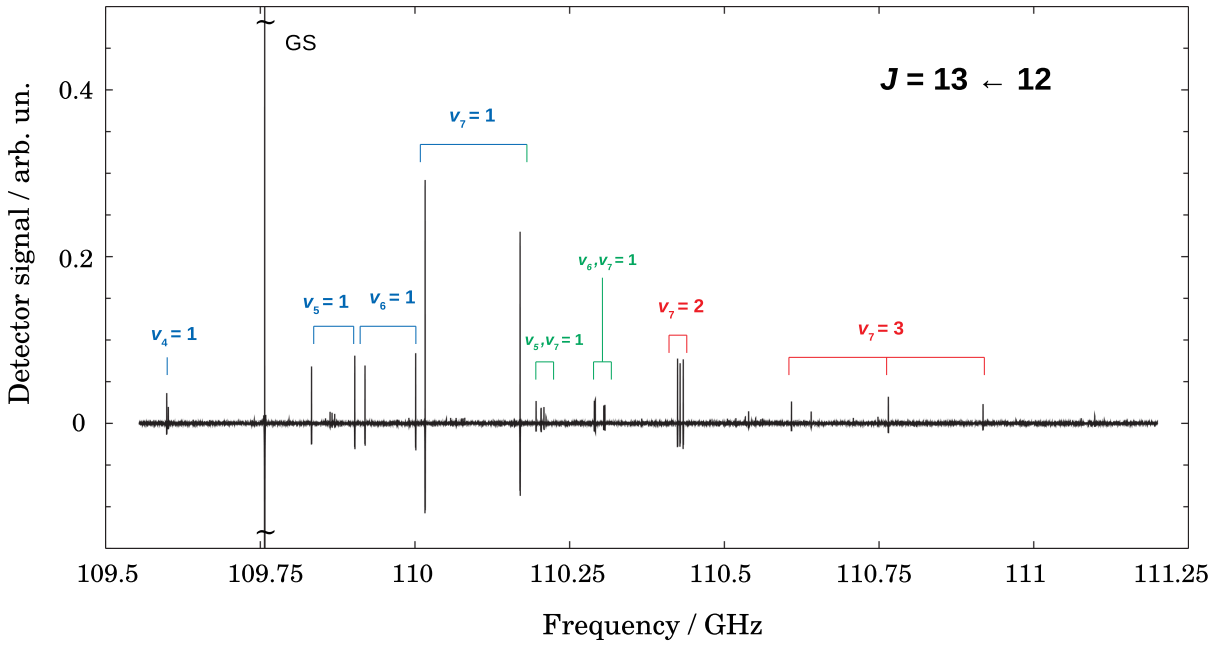

Figure 3: A 2 GHz broad scan of the $J = 13 \leftarrow 12$ rotational transition of DC_3N around 110 GHz. The spectrum was recorded at room temperature, with DC_3N at a pressure of 0.05 Pa, RC= 3 ms, frequency step 50 kHz, FM = 120 kHz, scan speed = 0.4 MHz/s, 2 scans. The arbitrary units of the y-axis are set so that the intensity of the ground state (GS) transition, out of scale in the figure, is 1.

Table 5: Spectroscopic constants derived for DC_3N in singly-excited bending states.

Constant	Unit	$v_7 = 1$	$v_6 = 1$	$v_5 = 1$
G_v	cm^{-1}	211.5502859(33)	492.7605681(48)	522.2639331(49)
$X_{L_{(tt)}}$	GHz	19.5125[a]	56.39[a]	...
B_v	MHz	4234.519466(31)	4229.25208(11)	4225.835835(71)
D_v	kHz	0.4718865(60)	0.462123(45)	0.452490(14)
H_v	mHz	0.08240(30)	0.0637(45)	0.03949[b]
L_v	nHz	−0.154[b]	−0.154[b]	−0.154[b]
$d_{JL_{(tt)}}$	kHz	−9.971[a]	141.5[a]	...
q_t	MHz	5.907823(56)	3.15095(11)	2.68903(13)
q_{tJ}	Hz	−13.646(11)	−1.572(22)	−1.627(27)
q_{tJJ}	µHz	43.37(57)	...	...

Number in parenthesis are one standard deviation in units of the last quoted digit. [a] Constrained value, see text. [b] Kept fixed to ground state value.

terms, $(v_4 = 1)$–$(v_6 = 2)$ and $(v_4 = 1)$–$(v_5 = v_6 = 1)$, and C_{50} for the quintic term $(v_4 = 1)$–$(v_7 = 4)$. Moreover, a centrifugal distortion parameter C_{50}^J was included in the analysis.

For the states involved in this resonance system, many experimental data are available. In the MIR region, we recorded the ν_4, $\nu_5+\nu_6$, and $2\nu_6$ bands that provide the energy position for most of the interacting levels. The energy of the $v_7 = 4$ was determined through the FIR spectrum, where the $4\nu_7 \leftarrow 3\nu_7$ hot-band

Table 6: Spectroscopic constants derived for DC_3N in overtone states.

Constant	Unit	$v_7 = 2$	$v_7 = 3$	$v_7 = 4$	$v_6 = 2$
G_v	cm^{-1}	422.3753581(61)	632.510162(64)	841.9860892(95)	983.021(78)
$X_{L_{(tt)}}$	GHz	19.354043(62)	19.1988(19)	19.03874(52)	56.39(58)
$y_{L_{(tt)}}$	MHz	...	...	1.82(12)	...
B_v	MHz	4247.45224(11)	4260.38118(15)	4273.30576(21)	4236.558(16)
D_v	kHz	0.491827(21)	0.512469(34)	0.53448(11)	0.471993(61)
H_v	mHz	0.03949[b]	0.03949[b]	0.176(21)	0.03949[b]
L_v	nHz	−0.154[b]	−0.154[b]	−0.154[b]	−0.154[b]
$d_{JL_{(tt)}}$	kHz	−10.426(30)	−10.947(24)	−11.368(21)	141.6(39)
$h_{JL_{(tt)}}$	Hz	...	...	−0.0552(64)	...
q_t	MHz	5.93258(10)	5.95888(12)	5.98281(15)	3.15095[a]
q_{tJ}	Hz	−13.897[a]	−14.149(36)	−14.288(46)	−1.571[a]
q_{tJJ}	µHz	43.37[a]	43.37[a]	43.37[a]	...

Number in parenthesis are one standard deviation in units of the last quoted digit. [a] Constrained value, see text. [b] Kept fixed to ground state value.

and the $4\nu_7 \leftarrow \nu_6$ band were detected. A large pure rotational data-set is also available for the polyad of interacting states. Besides several rotational transitions observed within the vibrational states, a small set of interstate transitions between the (1000) and (0004) states were identified. The coefficients C_{mn} of the resonance Hamiltonian are given in Table 8.

5. Conclusions

In this work, a large set of high-resolution rotational and ro-vibrational data of DC_3N has been recorded and analyzed in order to achieve a detailed knowledge of all the vibrational states approximately below 1000 cm^{-1} of energy. To reach this goal, infrared spectra of DC_3N have been recorded in the range 150–1600 cm^{-1} at high resolution (0.001–0.004 cm^{-1}). In this region, 27 fundamental, overtone, combination, and hot-bands have been observed and analyzed. Notably, the very weak ν_4 fundamental has also been detected, even though at lower resolution (0.012 cm^{-1}). Also, pure rotational transitions for 14 states have been recorded to extend the investigation of the spectrum to the submillimeter-wave region up to *ca.* 500 GHz.

Almost 6700 experimental transitions were included in a least-squares fit procedure thanks to which a large number of rotational and ro-vibrational spectroscopic parameters have been determined for 14 different vibrational states. The whole set of data has been fitted with an overall weighted standard deviation σ of 0.95, meaning that on average all data are well-reproduced within their given uncertainties. The vibrational energies were determined experimentally for all the investigated states, without any assumption. The combination of both high-resolution ro-vibrational data and pure rotational measurements allowed an accurate modeling of the spectrum of DC_3N, including perturbations produced by the observed anharmonic resonances. The interaction between the (1000) and (0110) states has been introduced for the first time, with the effect to eliminate the residual discrepancies described in Refs. [18, 25].

The present work shows once again the success of a combined analysis of data from different spectral regions, like infrared and millimeter-wave fields. The results are generally more coherent and fewer assumptions are needed, if not any. Also, a more extended set of spectroscopic parameters can be obtained with reliability.

This study provides an extensive line catalog (deposited as Supplementary Material) which can be used to assist future astronomical observations of DC_3N and is suitable for modeling both cold and hot regions

Table 7: Spectroscopic constants derived for DC_3N in combination states.

Constant	Unit	$v_6 = v_7 = 1$	$v_5 = v_7 = 1$	$v_5 = v_6 = 1$	$v_6 = 1, v_7 = 2$	$v_5 = 1, v_7 = 2$
G_v	cm^{-1}	703.8550157(95)	734.058721(13)	1014.2947(11)	914.21137(23)	945.143633(32)
$X_{L_{(aa)}}$	GHz	56.39[a]	...	...	56.39[a]	...
$X_{L_{(bb)}}$	GHz	19.3189[a]	19.5125[a]	56.39[a]	19.1254(87)	19.3142(16)
$X_{L_{(ab)}}$	GHz	16.16651(21)	23.13131(38)	40.245(33)	16.2848(57)	23.0216(30)
r_{ab}	GHz	−17.04625(41)	0.32219(69)	−63.498(67)	−16.6526(81)	0.87043(34)
r_{abJ}	kHz	−5.784(70)	−65.965(72)	...	−12.0(12)	−64.05(11)
B_v	MHz	4242.274182(83)	4238.741823(94)	4233.55575(16)	4255.2987(20)	4251.64459(18)
D_v	kHz	0.481887(24)	0.472594(28)	0.463447(40)	0.502237(37)	0.492993(33)
H_v	mHz	0.03949[b]	0.03949[b]	0.03949[b]	0.03949[b]	0.03949[b]
L_v	nHz	−0.154[b]	−0.154[b]	−0.154[b]	−0.154[b]	−0.154[b]
$d_{JL_{(aa)}}$	kHz	−11.254[a]	...	...	141.5[a]	...
$d_{JL_{(bb)}}$	kHz	141.5[a]	−9.971[a]	141.5[a]	−12.54(76)	−10.482(55)
$d_{JL_{(ab)}}$	kHz	43.88(12)	−5.08(13)	80.35(29)	43.75(46)	−6.810(46)
q_a	MHz	3.17827(15)	2.70634(31)	2.69091(31)	3.19092(20)	2.72654(16)
q_{aJ}	Hz	−1.571[a]	−1.626[a]	−1.626[a]	−1.517[a]	−1.626[a]
q_b	MHz	5.94427(18)	5.90943(73)	3.15095[a]	5.9489(16)	5.93169(23)
q_{bJ}	Hz	−13.646[a]	−13.738(98)	−1.571[a]	−14.17(33)	−13.646[a]
q_{bJJ}	µHz	43.37[a]	43.37[a]	...	43.37[a]	43.37[a]
u_{ab}	Hz	...	...	−1.641(74)	...	...

Number in parenthesis are one standard deviation in units of the last quoted digit. [a] Constrained value, see text. [b] Kept fixed to ground state value.

Table 8: Resonance parameters.

Interacting states	Parameter	Unit	Value
$(v_4 = 1)$ – $(v_6 = 2)$	C_{30}	cm^{-1}	17.422(33)
$(v_4 = 1)$ – $(v_5 = v_6 = 1)$	C_{30}	cm^{-1}	−6.527(13)
$(v_4 = 1)$ – $(v_7 = 4)$	C_{50}	GHz	2.70065(76)
	C_{50}^J	kHz	9.807(35)

Number in parenthesis are one standard deviation in units of the last quoted digit.

of the interstellar medium.

6. Acknowledgement

This study was supported by Bologna University (RFO funds) and by MIUR (Project PRIN 2015: STARS in the CAOS, Grant Number 2015F59J3R). This work has been performed under the SOLEIL proposal #20190128; we acknowledge the SOLEIL facility for provision of synchrotron radiation and would like to thank the AILES beamline staff for their assistance. L.B., P.C., and B.M.G. acknowledge the support by the Max Planck Society. V.M.R. has received funding from the European Union's Horizon 2020 research and innovation programme under the Marie Skłodowska-Curie grant agreement No 664931. LC acknowledges support from the Italian Ministero dell'Istruzione, Università e Ricerca through the grant Progetti Premiali 2012 - iALMA (CUP C52I13000140001). J.-C.G. thanks the Centre National d'Etudes Spatiales (CNES) for a grant.

References

[1] B. A. McGuire, 2018 Census of Interstellar, Circumstellar, Extragalactic, Protoplanetary Disk, and Exoplanetary Molecules, Astrophys. J. Suppl. S. 239 (2018) 17.
[2] S. Yamamoto, Introduction to Astrochemistry: Chemical Evolution from Interstellar Clouds to Star and Planet Formation, Springer, 2017.
[3] R. Loomis, et al., The third time's a charm? a rigorous investigation of spectral line stacking techniques and application to the detection of $HC_{11}N$, submitted.
[4] H. Suzuki, S. Yamamoto, M. Ohishi, N. Kaifu, S.-I. Ishikawa, Y. Hirahara, S. Takano, A survey of CCS, HC_3N, HC_5N, and NH_3 toward dark cloud cores and their production chemistry, Astrophys. J. 392 (1992) 551–570.
[5] F. Wyrowski, P. Schilke, S. Thorwirth, K. Menten, G. Winnewisser, Physical conditions in the proto-planetary nebula CRL 618 derived from observations of vibrationally excited HC_3N, Astrophys. J. 586 (1) (2003) 344.
[6] L. Decin, M. Agúndez, M. J. Barlow, F. Daniel, J. Cernicharo, R. Lombaert, E. De Beck, P. Royer, B. Vandenbussche, R. Wesson, et al., Warm water vapour in the sooty outflow from a luminous carbon star, Nature 467 (7311) (2010) 64.
[7] J. Li, J. Wang, Q. Gu, Z.-y. Zhang, X. Zheng, Large-scale kinematics, astrochemistry, and magnetic field studies of massive star-forming regions through HC_3N, HNC, and C_2H mappings, Astrophys. J. 745 (1) (2011) 47.
[8] E. Chapillon, A. Dutrey, S. Guilloteau, V. Piétu, V. Wakelam, F. Hersant, F. Gueth, T. Henning, R. Launhardt, K. Schreyer, et al., Chemistry in disks. VII. first detection of HC_3N in protoplanetary disks, Astrophys. J. 756 (1) (2012) 58.
[9] A. J. Al-Edhari, C. Ceccarelli, C. Kahane, S. Viti, N. Balucani, E. Caux, A. Faure, B. Lefloch, F. Lique, E. Mendoza, et al., History of the solar-type protostar IRAS 16293–2422 as told by the cyanopolyynes, Astron. Astrophys. 597 (2017) A40.
[10] F. Rico-Villas, J. Martin-Pintado, E. Gonzalez-Alfonso, S. Martin, V. M. Rivilla, Super hot cores in NGC 253: witnessing the formation and early evolution of super star clusters, Mon. Not. R. Astron. Soc. 491 (3) (2020) 4573–4589.
[11] S. Zeng, I. Jiménez-Serra, V. Rivilla, S. Martín, J. Martín-Pintado, M. Requena-Torres, J. Armijos-Abendaño, D. Riquelme, R. Aladro, Complex organic molecules in the Galactic Centre: the N-bearing family, Mon. Not. R. Astron. Soc. 478 (3) (2018) 2962–2975.
[12] W. Langer, F. Schloerb, R. Snell, J. Young, Detection of deuterated cyanoacetylene in the interstellar cloud TMC-1, Astrophys. J. 239 (1980) L125–L128.
[13] G. B. Esplugues, J. Cernicharo, S. Viti, J. R. Goicoechea, B. Tercero, N. Marcelino, et al., Combined IRAM and Herschel/HIFI study of cyano(di)acetylene in Orion KL: tentative detection of DC_3N, Astron. Astrophys. 559 (2013) A51.

[14] A. Belloche, H. Müller, R. Garrod, K. Menten, Exploring molecular complexity with ALMA (EMoCA): Deuterated complex organic molecules in Sagittarius B2 (N2), Astron. Astrophys. 587 (2016) A91.
[15] E. Bianchi, C. Ceccarelli, C. Codella, J. Enrique-Romero, C. Favre, B. Lefloch, Astrochemistry as a tool to follow protostellar evolution: The class I stage, ACS Earth Space Chem. 3 (12) (2019) 2659–2674.
[16] V. M. Rivilla, L. Colzi, F. Fontani, M. Melosso, P. Caselli, L. Bizzocchi, F. Tamassia, L. Dore, DC_3N observations towards high-mass star-forming regions, Mon. Not. R. Astron. Soc.Staa1616. arXiv:https://academic.oup.com/mnras/advance-article-pdf/doi/10.1093/mnras/staa1616/33371666/staa1616.pdf, doi:10.1093/mnras/staa1616.
URL https://doi.org/10.1093/mnras/staa1616
[17] P. Mallinson, R. L. de Zafra, The microwave spectrum of cyanoacetylene in ground and excited vibrational states, Mol. Phys. 36 (3) (1978) 827–843.
[18] G. Plummer, D. Mauer, K. Yamada, K. Möller, Rotational spectra of DC_3N in some excited vibrational states, J. Mol. Spectrosc. 130 (2) (1988) 407–418.
[19] H. Spahn, H. S. Müller, T. F. Giesen, J.-U. Grabow, M. E. Harding, J. Gauss, S. Schlemmer, Rotational spectra and hyperfine structure of isotopic species of deuterated cyanoacetylene, DC_3N, Chem. Phys. 346 (1-3) (2008) 132–138.
[20] E. Fliege, H. Dreizler, B. Kleibömer, Deuterium and nitrogen quadrupole coupling in cyanodeuteroacetylene, J. Mol. Struct. 97 (1983) 225–228.
[21] L. Tack, S. G. Kukolich, Beam-maser spectroscopy on cyanoacetylene-D, J. Chem. Phys. 78 (11) (1983) 6512–6514.
[22] M. Uyemura, S. Deguchi, Y. Nakada, T. Onaka, Infrared intensities of bending fundamentals in gaseous HCCCN and DCCCN, Bull. Chem. Soc. Jpn. 55 (2) (1982) 384–388.
[23] Y. Bénilan, A. Jolly, F. Raulin, J.-C. Guillemin, IR band intensities of DC_3N and $HC_3^{15}N$: Implication for observations of Titan's atmosphere, Planet. Space Sci. 54 (6) (2006) 635–640.
[24] P. Mallinson, A. Fayt, High resolution infra-red studies of HCCCN and DCCCN, Mol. Phys. 32 (2) (1976) 473–485.
[25] B. Coveliers, W. Ahmed, A. Fayt, H. Bürger, Far-infrared spectra of DCCCN, J. Mol. Spectrosc. 156 (1) (1992) 77–88.
[26] J.-B. Brubach, L. Manceron, M. Rouzières, O. Pirali, D. Balcon, F. Kwabia-Tchana, V. Boudon, M. Tudorie, T. Huet, A. Cuisset, P. Roy, Performance of the AILES THz-Infrared beamline at SOLEIL for High resolution spectroscopy, in: WIRMS 2009, Vol. 1214 of AIP Conference Proceedings, 2010, pp. 81–84.
[27] O. Pirali, V. Boudon, J. Oomens, M. Vervloet, Rotationally resolved infrared spectroscopy of adamantane, J. Chem. Phys. 136 (2012) 024310.
[28] O. Pirali, M. Goubet, T. R. Huet, R. Georges, P. Soulard, P. Asselin, J. Courbe, P. Roy, M. Vervloet, The far infrared spectrum of naphthalene characterized by high resolution synchrotron FTIR spectroscopy and anharmonic DFT calculations, Phys. Chem. Chem. Phys. 15 (25) (2013) 10141–10150. doi:10.1039/c3cp44305a.
[29] F. Tamassia, M. Melosso, L. Dore, M. Pettini, E. Canè, P. Stoppa, A. Pietropolli Charmet, Spectroscopy of a low global warming power refrigerant. infrared and millimeter-wave spectra of trifluoroethene (HFO-1123) in the ground and some vibrational excited states, J. Quant. Spectrosc. Ra. 248 (2020) 106980. doi:10.1016/j.jqsrt.2020.106980.
[30] F. Matsushima, H. Odashima, T. Iwasaki, S. Tsunekawa, K. Takagi, Frequency-measurement of pure rotational transitions of H_2O from 0.5 to 5 THz, J. Mol. Struct. 352 (1995) 371–378.
[31] V. M. Horneman, R. Anttila, S. Alanko, J. Pietila, Transferring calibration from CO_2 laser lines to far infrared water lines with the aid of the ν_2 band of OCS and the ν_2, ν_1- ν_2, and ν_1+ ν_2 bands of $^{13}CS_2$: Molecular constants of $^{13}CS_2$, J. Mol. Spectrosc. 234 (2) (2005) 238–254.
[32] I. E. Gordon, L. S. Rothman, C. Hill, R. V. Kochanov, Y. Tan, P. F. Bernath, M. Birk, V. Boudon, A. Campargue, K. Chance, et al., The HITRAN2016 molecular spectroscopic database, J. Quant. Spectrosc. Ra. 203 (2017) 3–69.
[33] C. Degli Esposti, M. Melosso, L. Bizzocchi, F. Tamassia, L. Dore, Determination of a semi-experimental equilibrium structure of 1-phosphapropyne from millimeter-wave spectroscopy of CH_3CP and CD_3CP, J. Mol. Struct. 1203 (2020) 127429.
[34] M. Melosso, L. Dore, F. Tamassia, C. L. Brogan, T. R. Hunter, B. A. McGuire, The sub-millimeter rotational spectrum of ethylene glycol up to 890 GHz and application to ALMA Band 10 spectral line data of NGC 6334I, J. Phys. Chem. A 124 (2020) 240–246.
[35] L. Bizzocchi, V. Lattanzi, J. Laas, S. Spezzano, B. M. Giuliano, D. Prudenzano, C. Endres, O. Sipilä, P. Caselli, Accurate sub-millimetre rest frequencies for $HOCO^+$ and $DOCO^+$ ions, Astron. Astrophys. 602 (2017) A34.
[36] J. Brown, J. Hougen, K.-P. Huber, et al., The labeling of parity doublet levels in linear molecules, J. Mol. Spectrosc. 55 (1-3) (1975) 500–503.
[37] K. M. Yamada, F. Birss, M. Aliev, Effective Hamiltonian for polyatomic linear molecules, J. Mol. Spectrosc. 112 (2) (1985) 347–356.
[38] L. Bizzocchi, F. Tamassia, J. Laas, B. M. Giuliano, C. Degli Esposti, L. Dore, et al., Rotational and high-resolution infrared spectrum of HC_3N: Global ro-vibrational analysis and improved line catalog for astrophysical observations, Astrophys. J. Suppl. Ser. 233.
[39] H. M. Pickett, The fitting and prediction of vibration-rotation spectra with spin interactions, J. Mol. Spectrosc. 148 (2) (1991) 371–377.